CrossMark

ORIGINAL ARTICLE

Numerical experiments with RAMS model in highly complex terrain

A. Balanzino[1] · S. Trini Castelli[1] (ID)

Abstract RAMS mesoscale model has been applied to simulate the atmospheric circulation in highly complex terrain, in the Hindu-Kush Karakorum and Himalaya regions. The goal of the work is to assess the sensitivity of the model to the grid spacing and related resolution, the smoothing of the orography, the microphysics parameterizations, in such heterogeneous and challenging conditions. As a follow up, the capability of the model in correctly capturing the atmospheric processes is tested. Two main cases, where some measured data were available, have been considered: a period during which a flood occurred and a period characterised by high-pollution episodes. RAMS model provided sensible results, the predictions reasonably reproduce the observed data at a regional scale, but the most local characteristics cannot be definitely described even at the typical resolution of 1 km order.

Keywords Complex terrain · Mesoscale models · Grid spacing · Model resolution · Sensitivity tests

1 Introduction

Mountain regions represent an environment and ecosystem particularly sensitive and very responsive to changes. The scientific community is engaged in several international and national research programmes related to the study and protection of mountainous areas (see, for instance, http://belmontforum.org/cra-2015-mountains-as-sentinels-of-change and

✉ S. Trini Castelli
s.trinicastelli@isac.cnr.it

1 Institute of Atmospheric Sciences and Climate – National Research Council (ISAC-CNR), Corso Fiume 4, 10133 Turin, Italy

ⓈSpringer

http://www.nextdataproject.it/). A major issue linked to this scientific topic is to perform meteorological and climatological simulations that can be accurate enough to correctly represent and predict the atmospheric and environmental processes in such complex and heterogeneous topography.

For reproducing the meteorological conditions in mountainous areas, mesoscale models are the main choice, simulating the atmosphere at horizontal scales ranging from a few kilometres to several hundred kilometres, with a typical resolution up to the order of 1 km. The main advantage of this kind of models in highly inhomogeneous terrain is their ability to account effectively for the influences of topography on the flow field, resolving valley and slope winds. Mesoscale models are usually driven by the meteorological fields obtained from global models (such as the analyses of the *European Centre for Medium Range Weather Forecast*, ECMWF, and of the *National Centers for Environmental Prediction*, NCEP), representing the synoptic-scale influence. At the same time, thanks to the grid-nesting technique, they can run with horizontal resolutions high enough to reproduce also the main features of the local meteorology. The mesoscale and local scale circulations are related to the presence of main and lateral valleys, ridges and land-use heterogeneity, and they superimpose over the large-scale circulation. Typical features are air stagnation regions in the lee of obstacles, separation of the flow and differentially heated valley slopes. To reproduce correctly the meteorology of the region of interest, also the forcing of the synoptic circulation has to be taken into account, possibly describing the interaction between the large-scale processes and the local and small-scale ones. Driving the regional models by general circulation model outputs is thus the common approach for this purpose. Then, the nesting technique, coupled with high-resolution domain meshes, allows downscaling from typical mesoscale to local scales. This is particularly important in the assessment of atmospheric pollution, which involves a lot of physical processes and possible problems, related to the distinctive features of both the meteorology and dispersion in complex topography. A thorough discussion on these aspects is presented in Heimann et al. [11] and Arnold et al. [1].

Several studies in the Alpine regions proved that in highly complex orography certain terrain-induced meteorological processes cannot be captured until 1-km or finer resolutions are used. Looking back at last decade, Gohm et al. [7] assessed to what extent the MM5 model [8], run at a very high horizontal grid spacing, up to 267 m, was able to simulate the temporal evolution and spatial structure of small-scale orographic flows, in application to the dynamics of foehn winds in an Alpine valley. The importance of a proper resolution of the model topography and of advanced boundary layer parameterization schemes was defined. MM5 was applied by Zängl et al. [31] also to address the capability of mesoscale models in reproducing the distinctive features of the foehn, investigating the dependence of the model performance on the horizontal grid resolution. At the high resolution of 800 m most of the observed features were well reproduced, while the results deteriorated for 1.4 km resolution. Both analyses were conducted based on observations collected during the Mesoscale Alpine Programme (MAP [3]). A comprehensive discussion, summarizing the key findings related to observational and modelling investigation of the boundary-layer structure in complex terrain for MAP and other field campaigns, is proposed by Rotach and Zardi [18]. Trini Castelli et al. [23] compared hydrostatic ETA [13] and non-hydrostatic RAMS [4, 14] models, based on observations from TRACT field campaign (TRansport of pollutants over Complex Terrain [21]), at different resolutions to assess their ability in correctly reproducing the flow fields in complex terrain, with the final aim of using them to drive air pollution dispersion models. De Wekker et al. [5] assessed the performance of RAMS, run at a horizontal grid spacing up to 330 m, in reproducing convective boundary

layer structure in a steep valley and in predicting the wind and temperature fields, the convective boundary layer height and surface sensible heat fluxes, referring to the MAP-Riviera field study [17]. Higher horizontal grid spacing, up to 250 m, was adopted in RAMS model to investigate the performances of alternative boundary-layer and turbulence parameterization in capturing both the flow features [24] and the dispersion of pollutants [10] in coastal complex terrain, in the Tsukuba region (Japan). Different modelling systems were applied and tested at high resolutions during the ALPNAP Alpine Space Project [11, 19, 25, 26], to investigate and describe the characteristics of the air pollutants dispersion and noise propagation in the European Alpine valleys and to provide science-based methods and tools for monitoring and predicting the environmental impact. More recently, Wagner et al. [27] studied the influence of the horizontal model grid resolution on the boundary layer structure over an idealized valley, to investigate how the atmospheric flows over complex terrain differ when the topography in the numerical model is fully resolved, smoothed, or unresolved. In their work, the WRF-ARW model [20] was used and its grid size was gradually decreased from LES (Large-Eddy Simulation) high resolution, with 50 m grid spacing, to coarse resolution typical of hydrostatic modelling, 10 km. Arnold et al. [1] provide an overview of the problems related to high-resolution simulations in complex terrain with mesoscale models. Key aspects, like computational and numerical issues, the accuracy and representativeness of initialisation and input data (land use, topography, surface variables etc.), the applicability of boundary-layer parameterizations for heterogeneous conditions, are thoroughly investigated and discussed, drawing possible approaches to address them.

In this context, the present work is aimed at investigating and assessing the capability of mesoscale models in correctly characterizing the local and typical meteorology in the very complex orography and high altitudes of Hindu-Kush Karakorum and Himalaya regions (HKKH hereafter). Mesoscale model simulations in the Himalayan region (Kali Gandaki Valley, Nepal) were performed by Zängl et al. [30] to support the interpretation of meteorological observations, collected for studying the circulation processes in such highly complex topography. MM5 model was used up to a resolution of 800 m. Also Regmi et al. [16] used MM5, with a finest resolution of 1 km, to investigate the prevailing local meteorological condition in late wintertime in the Kathmandu valley. The simulated flow fields were used for studying and interpreting the distribution of the atmospheric pollutants in the area.

The scientific literature related to high-resolution simulations in these complex and remote areas is certainly not vast, due to limited available observations too. This work can bring a contribution to the assessment of mesoscale models applied in extremely complex topography, where differences in altitude vary up to 6000 m.

For this purpose, high-resolution simulations have been performed, also considering extreme meteorological conditions and air pollution episodes. The main results of numerical experiments are presented and discussed here. A comprehensive and technical report on the related research activity, carried out in the framework of RECCO Special Project (REgional Climate in Complex Orography) in the National Project of Interest NextData (http://www.nextdataproject.it/), is given in Balanzino and Trini Castelli [2].

Here, two case studies are considered.

Case Study I a critical episode related to a flood, in the period 24–31 July 2010 [6, 12, 22, 28]. Here the interest lays in investigating the capability of the model to capture an extreme meteorological episode.

Case Study II an episode of high air pollution related to the specific atmospheric circulation in the region in the period from 20 August to 10 November 2012 [15]. The rationale of this study is to assess the capability of the model to capture the atmospheric conditions and to provide representative high-resolution meteorological fields, which can be of support to related air pollution studies and their impact assessment.

We present details and examples of the simulations focusing on their sensitivity to grid resolution, orography representation, level of the microphysics parameterization.

The main questions we want to address are: (1) Is the model able at such resolutions in such complex terrain to provide reliable outputs? (2) How accurate is it to extract by interpolation the meteorological variable at a station, in such complex areas? (3) What are the noticeable consequences of considering interpolated data to evaluate the model predictions against the observations?

The simulations were performed with the latest version 6.0 of RAMS model (Regional Atmospheric Modeling System [4, 14]), briefly described in Sect. 2. In Sects. 2 and 3 we investigate the sensitivity of the model to the parameterizations chosen respectively to treat the orography and, for Case Study I, to solve the microphysics. In Sect. 4 the model performances in complex terrain for different resolution is assessed for Case Study II. Conclusions are drawn in Sect. 5.

The results of the model simulations are evaluated using the available observed data, collected at stations in different locations. It is worth reminding some general considerations for a proper understanding of this kind of comparison. First of all, model outputs are volume averages defined by the horizontal and vertical grid spacing Δx, Δy, Δz used in the simulated domain and they refer to mean quantities, while the observations are instantaneous and single-point values that may significantly differ from the volume averages. In addition to this, the measuring sites are generally located in heterogeneous areas that can be not fully resolved at the grid scale, in particular because in complex terrain the orography used in the simulations is generally smoother than the real orography, so that the altitudes of the measuring point and the simulation grid points may be significantly different. Therefore, due to the smoothed nature of the simulation results, the finer structure in the observed profiles cannot be fully captured.

On their side, the observed meteorological variables are affected by fundamental stochastic uncertainty: according to many authors and to our experience too, a variability of hourly averaged wind speed of the order of 1–2 ms^{-1} over distances of a few kilometres can be observed even on flat homogeneous terrain, due to mesoscale turbulence fluctuations. Moreover, instrumentation and averaging errors, unavoidable in any measurements, can affect this kind of paired comparisons.

For all these reasons, a precise point-to-point agreement between observed and predicted data cannot be expected and a good result is obtained when the mean trend of measurements is reproduced by the simulated variables.

To produce the simulated fields at a surface station, it is common use to interpolate the values simulated at the grid points surrounding its location, possibly applying also a vertical interpolation from the closest model levels to the measuring height. This is a known critical issue when dealing with highly complex topography and land-use heterogeneity. Here we compare the observations to the predicted data of the first model level at the four grid points around the station, in order to highlight the possible differences due to the different altitudes of the points. To investigate such issue, in some cases we compare these plots with the interpolated values at the same location.

We note that all results are presented in UTC hours. This has to be accounted for when discussing the local daily cycle depending on the season and on the location, corresponding to 5 h more in the HKKH local time.

2 Numerical simulations and related observed data

RAMS [4, 14] is a non-hydrostatic model, originally developed from a mesoscale model and a cloud model at the Colorado State University. RAMS is designed to simulate a large range of atmospheric flows in a wide spectrum of scales, from local and regional to synoptic. It may be configured to cover an area as large as a hemisphere or to simulate microscale phenomena, since in principle there are no lower limits in the domain size or in the model grid cell size. The model includes a large number of options for the simulation of the atmospheric processes. The main features are hydrostatic and non-hydrostatic mode, two-way interactive grid nesting, terrain-following coordinates, stretched vertical coordinates, nudging system, different options for numerical schemes, several upper and lateral boundary conditions and a set of parameterisations for the physical processes. RAMS includes a model for soil and vegetation temperature and moisture. To read and process the output meteorological variables we used the RAMS post-processing package REVU (RAMS Evaluation and Visualization Utilities).
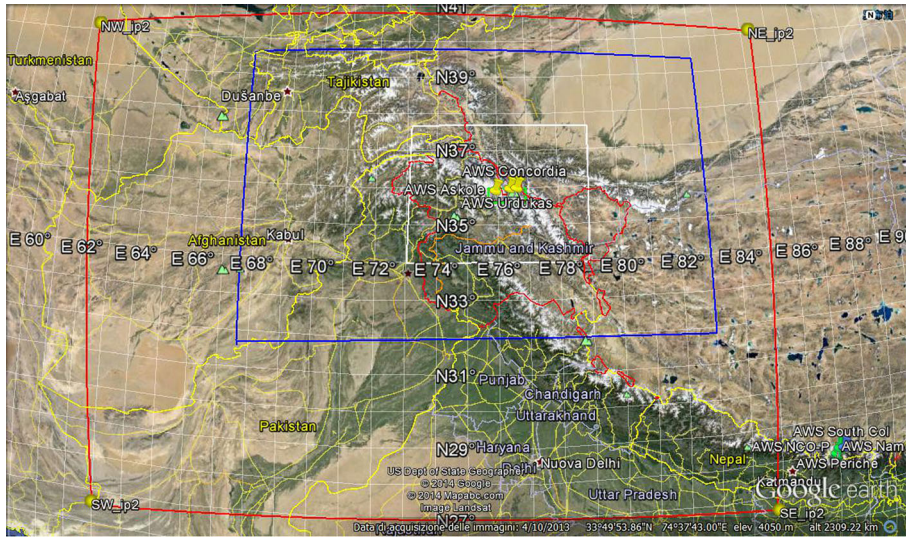
2.1 Configuration of the simulation

In the RAMS model, the two-way grid nesting interactive procedure provides an interactive 'zoom' from large-scale area to smaller scale domains, and the non-hydrostatic option allows representing all meteorologically relevant spatial scales. In particular, the two-way nesting procedure allows optimising the interaction between the different scales. The simulations were thus configured using four nested grids with a horizontal grid spacing of 64, 16, 4 and 1 km, respectively: the main outer one covers a wide domain, where the main large scale topographical features of the HKKH region are included. The next two intermediate grids zoom over the area of interest and they are chosen to be compatible with the main local topographic features (Fig. 1). The last domain, having the highest resolution, is focused over the HKKH area where the observational stations were located and have been selected for the NextData-RECCO Project. The 3D configuration of the four grids is described in Table 1.

The initialisation of the RAMS model is obtained from the ECMWF analyses with a resolution of 0.5° (that is, at middle latitudes, about 50 km). In input to RAMS, the large-scale 3D meteorological fields give the initial conditions and the boundary conditions that drive the model during the simulation by means of the nudging technique.

2.2 The available observations

The modelling activities are focused on the Central Karakorum National Park (on Baltoro Glacier). In this region, three Automatic Weather Stations (AWS) are installed in the villages of Askole, Urdukas and in Concordia site. Askole station is on the lower, southern part of the moraine platform, near the edge above the river. It is located in the middle of a crop area and has unobstructed view toward East (valley upward), West (valley downward), South (in front of opposite side of the valley) and North (leading to the slopes of the

Fig. 1 Simulation domains (four nested grids) with the considered measuring stations in yellow

Table 1 3D configurations of the four nested grids used in RAMS

	GRID1	GRID2	GRID3	GRID4
Horizontal dimension (km)	2112 × 1728	1488 × 912	340 × 228	105 × 45
Horizontal grid spacing (km)	64 × 64	16 × 16	4 × 4	1 × 1
Number of vertical levels	27	27	27	27
Top of the domain (m)	19,251.3	19,251.3	19,251.3	19,251.3
Number of x gridpoints (W-E)	34	94	86	106
Number of y gridpoints (N-S)	28	58	58	46
Centre latitude (°)	34	36.2905	36.1425	35.7961
Centre longitude (°)	74	75.7856	76.0497	76.3071
SW point (LAT,LON) (°)	(25.803, 63.506)	(32.045, 67.802)	(35.134, 74.154)	(35.603, 75.721)
NE point (LAT,LON) (°)	(41.126, 86.573)	(39.948, 84.586)	(37.120, 77.992)	(35.986, 76.896)

mountain surrounding the village). Urdukas station is installed on a moraine ridge close to the left glacier margin. Concordia station is installed in the upper Baltoro Glacier, towards the top, to provide information about meteorology in the accumulation area of the glacier.

Observed data were available to us for the Case Study II (25/08–05/09/2012) for Askole and Concordia sites. We use here the temperature T (°C), the relative humidity RH (%), the wind speed WS (m s^{-1}) and wind direction WD (°), this last provided only for Askole station.

For Case Study I (24–31/07/2010) we considered seven stations of the Pakistan Meteorological Department (PMD), providing observed values for the daily temperature minimum and maximum and the daily mean rainfall. Four of these stations are inside the inner Grid 3 domain at 4-km grid-spacing, thus comparison are presented for them. For each station, we summarize the main characteristics in Table 2.

Code	Name	Lon (°E)	Lat (°N)	Altitude (m)	In grids
8	Askole	75.815	35.681	3015	1, 2, 3, 4
9	Urdukas	76.286	35.728	3926	1, 2, 3, 4
10	Concordia	76.514	35.744	4700	1, 2, 3, 4
14	Astore	74.9	35.33	2168	1, 2, 3
15	Skardu	75.68	35.30	2317	1, 2, 3
16	Gupis	73.40	36.17	2156	1, 2
17	Chitral	71.83	35.85	1498	1, 2
18	Gilgit	74.33	35.92	1460	1, 2, 3
19	Bunji	74.63	35.67	1372	1, 2, 3
20	Chilas	74.10	35.42	1250	1, 2

Table 2 Coordinates of the measuring stations in HKKH area: AWS stations (code number: 8–10) and PMD stations (code-number: 14–20)

For the comparison with observed data and for the discussion of the results sometimes we will consider the four grid points around the stations, other times we will consider the closest point, for all coordinates, and in other cases we will use values interpolated from RAMS outputs on the station location.

2.3 Comparing predictions and observations in highly complex terrain

Modelling systems generally offer their own post-processing packages to extract variables at stations or given points. We notice that when extrapolating the variables from RAMS outputs with its post-processing option, the final coordinates of the model point selected for the comparison are displaced with respect to the longitude and latitude of the measuring station given in input, therefore possibly spoiling the correctness of the comparison itself. In RAMS case, this can be ascribed to the passage from the geographical system to the coordinates in metres that is used, which are afterwards transformed in latitude and longitude again, producing the small difference with respect to the real ones and leading to an imprecise final positioning of the selected points. This inaccuracy adds on the unavoidable difference between the actual station altitude and the smoothed orography altitude used in RAMS simulation. In complex terrain, this effect is emphasized and the change in altitude has to be clearly taken into account when discussing the results. Using the extrapolation option in all grids for the values at the station locations, we found a non negligible difference between the actual station altitude and the one at the selected point. For instance, Urdukas (3926 m) is found to have an altitude of 5155 m in grid 1, 5400 m in grid 2, 4400 m in grid 3 and 4113 m in grid 4 (see also next Table 3 for Askole and Concordia). This issue leads to a well-known warning, which is to treat with particular care the comparison between observations and predictions from model simulations especially in complex terrain, to avoid misinterpreting the results and to assure that correct conclusions are drawn.

Such problem does not rise in a qualitative evaluation, where we compare outputs predicted by different simulations at the same selected point in the domain. It would instead affect a comparison with observed data. For this reason, when simulations are compared to observations, we generally consider the four grid points around the station, in order to have a glance on the variability in the predicted meteorological variables associated to the topographical complexity of the region.

Table 3 Altitudes (m) of the points corresponding to Askole and Concordia stations, using the interpolation option, in the four gridded domains for the different averaging options for topography

	Orography option	Grid 1	Grid 2	Grid 3	Grid 4
Askole 3015 m	OR0	4345	4380	4412	3423
	OR1	4558	4466	4479	3486
	OR2	4561	4497	4517	3521
	OR3	4349	4376	4433	3399
Concordia 4700 m	OR0	5056	5243	4968	4585
	OR1	5241	5280	5013	4603
	OR2	5231	5320	5038	4613
	OR3	5051	5248	4974	4579

To evaluate the sensitivity to the orography, we performed one-day simulations in the period of interest for the two case studies, on 21.07.2010 for Case Study I and 26.08.2012 for Case Study II. In RAMS, four different options are available for smoothing the orography [29]: *Average Orography (OR0)* where a conventional mean is computed; *Silhouette Orography (OR1)*, which adds mass by filling in valleys and it is used to maintain the effective mean barrier height that air must rise to when crossing a topographic barrier such as a ridge; *Envelope Orography (OR2)*, which is an alternative method of attempting to preserve barrier heights; *Reflected Envelope Orography (OR3)*, which aims at preserving both barrier heights and valley depths, leading to the steepest topography in RAMS, while still filtering the shortest wavelengths. We analysed the resulting topography for all cases. The orography values from OR0 and OR3 are the most similar, with a slight tendency to provide higher values for OR3, with the ratio OR0/OR3 mostly varying between 0.99 and 1.01. The approaches OR1 and OR2 tend instead to provide higher values of the altitude than OR3, for the full range of altitudes. This is connected to the fact that the effective mean barrier height is preserved but the valley depth is not, producing an average shift of the altitude to higher values. As example, the altitudes of the Askole and Concordia points at the four grids and for all options are reported in Table 3.

An estimate of the effect that these differences induce on the meteorological variables was performed comparing, also with the available observed data, the outputs of two simulations, the first using the "smooth" *Average* option OR0 and the second with the more "complex" *Reflected Envelope* option OR3, which showed the most similar trend to OR0. The main effect is seen for the wind speed, while the simulations are less sensitive to differences in the orography for the temperature and relative humidity. Major drifts between the two runs occur during daytime, where the difference in slopes and peaks due to the smoothing can play a fundamental role on the radiative effects and the consequent heating of the surfaces, affecting thus the temperature field, the circulation in the valley, the mountain-valley flow and breeze. In general, a certain scatter characterizes the temperature data, up to an order of ± 1 °C for temperatures below 10 °C in Grid 4. Above this temperature value, the simulation with a more complex orography OR3 provides values that are slightly higher than the ones obtained with a smoother orography scheme OR0. Wind speed values may show substantial differences for the two cases in the finest Grid 4, up to around ± 2 m s^{-1}. The spread is larger for the lower wind speeds.

The analysis shows that the smoothing of the orography may have a non-negligible effect on the reproduction of the meteorological fields, even when the differences between the altitudes is small, especially when high resolutions are used. A more realistic representation of the topographical characteristics, which means a lower level of smoothing, should be anyway applied. For maintaining as much as possible the correspondence between the real and the model topographies, as in past case studies we made the choice to adopt the *Reflected Envelope Orography* approach for next simulations.

3 Case Study I: sensitivity to the microphysics

In Case Study I, RAMS simulations were run for the entire selected period during which the flood occurred, from 24 to 31.07.2010.

In particular, the effect of the microphysics parameterization was investigated.

In RAMS, there are four options [29], described hereafter, for parameterizing the microphysics, determined by the level of their complexity, that is to what extent the moisture and precipitation processes are treated.

- LEVEL 0 causes the model to run dry, completely eliminating any process which influences or is influenced by any phase of moisture. With this option, radiation parameterizations must be turned off.
- LEVEL 1 activates advection, diffusion, and surface flux of water, where all water substance in the atmosphere is assumed to occur as vapour even if supersaturation occurs. The value of 1 also activates the buoyancy effect of water vapour in the vertical equation of motion, as well as the radiative effects of water vapour if radiation is activated elsewhere.
- LEVEL 2 activates condensation of water vapour to cloud water wherever supersaturation is attained. The partitioning of the total water substance into vapour and cloud water is purely diagnostic in this case. No other forms of liquid or ice water are considered. Both the positive buoyancy effect of water vapour and the liquid water loading of cloud water are included in the vertical equation of motion. Radiative effects of both water vapour and cloud water are activated, if the radiation parameterization is itself activated.
- LEVEL 3 activates the bulk microphysics parameterization, which includes cloud water, rain, pristine ice, snow, aggregates, graupel, and hail, or certain subsets of these. This parameterization includes the precipitation process.

Simulations were performed adopting both a complete microphysics parameterization (LEVEL 3), named as CS_I_MP3, and a simplified microphysics parameterization (LEVEL 2), named as CS_I_MP2. Comparisons with observed data have been carried out at the PMD stations because precipitation measurements are available only for these stations.

In the following graphs, we report the model results for the period 24–31.07.2010 for the four stations of Astore, Skardu, Gilgit and Bunji. The predicted values are taken at the grid points around the stations in Grid 3, since the stations are located outside the finest Grid 4 (see also Table 2). We compare the simulated temporal evolution of the temperature with the corresponding daily-observed maximum and minimum values, and the resolved surface precipitation, defined as "the average volume of water in the form of rain, snow, hail, or sleet that falls per unit of area and per unit of time at the site", with their mean

daily observed rainfall. The relative humidity is also considered, but no observed data were available for comparison.

In Grid 3, the following cases take place:

1. the latitude of Skardu and Bunji stations coincides with a latitude of the grid mesh, therefore only two grid-points where the longitudes are the closest to the station one, are considered;
2. the longitude of Astore and Gilgit stations coincides with a longitude of the grid mesh, therefore only two grid-points where the latitudes are the closest to the station one, are considered.

In addition to the values at these grid points, for the precipitation we plot also the simulated curve obtained by interpolating the variables from the grid points to the station site. This can highlight which is the dominant relative contribution of the different grid points.

In Fig. 2 we observe that, at all stations, the simulated temperature trends of CS_I_MP2 and CS_I_MP3 practically overlap until the 28th of July 2010 at 12:00 UTC and then they start differentiating. CS_I_MP2 run maintains the classic daily temperature cycle, computed values about 15 °C early in the morning and peaks of 20–25 °C at noon, and the temperature values are higher than for the CS_I_MP3 case in the last few days. In CS_I_MP3, instead, the model reproduces a perturbation, detected also by the observations as a sudden drop in the temperature maximum values. The observed data seem to reveal the occurrence of a heat wave, not captured by the model, in the days before the flood, during which then the temperatures drop to lower values. The CS_I_MP2 run cannot capture the precipitation event due to the approximation in the parameterization scheme, thus the perturbation and lowering of temperature recorded between the 28 and the 30 of July are not reproduced in this case. For all stations the temperature trend sets generally closer to the minimum observed values, getting far lower values than the maxima in the first 5 days, while in the last three ones, when the flood occurs, the agreement is better. Only for Skardu station, the agreement is fair. We notice, however, that the two Grid-3 points close to Astore station, at 2168 m, have a much higher altitude, respectively 3781 and 3726 m, resulting in more than 1500 m difference. Similar considerations hold for Gilgit (real altitude: 1460 m, grid points: 2366 and 2127 m) and Bungji (real altitude: 1372 m, grid points: 2132 and 1945 m) stations. Instead, the grid points around Skardu, 2317 m altitude, are placed at closer altitudes, 2532 m and 2745 m. The differences in altitudes at the four PMD stations and the grid points around them may be certainly decisive in determining the differences in the temperature values. This fact is better understood by looking at the position of the stations on maps (as shown in Figures SM1 and SM2 in the Online Resources), which highlight the extremely complex topography surrounding the stations themselves: in a range of 2 km radius, meteorological variables take certainly different values, especially in extreme conditions. Therefore, the simulated values in this case might be poorly representative of the local conditions at the measuring stations, given the relatively coarse 4-km horizontal resolution of Grid 3. Since we have no information on the quality of the observed data and on the setting of the measuring stations, such as possible direct exposure of the sensors to the sun rays, we cannot provide a more precise interpretation of the rather high maxima recorded for the temperature. We may expect that the values calculated on higher-resolution grids can be more adequately representative of the variables at a specific location, given their closer proximity, when the altitude is not much different.

As indicative examples (no observations available), in Fig. 3 we show the comparison between the relative humidity trends, at the four PMD stations included in Grid 3 using the
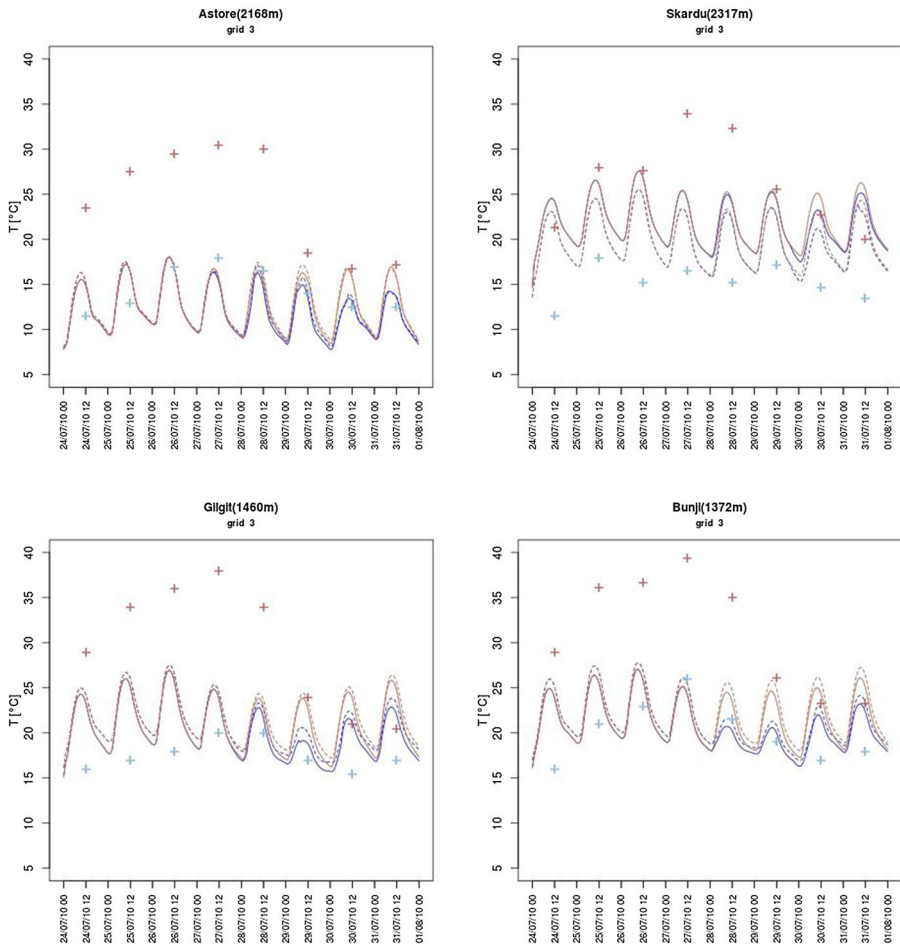
Fig. 2 Case Study I. Grid 3. Time evolution of the simulated temperature at the two grid points closest to the PMD stations (distinguished by solid and dashed lines), using two different microphysics parameterizations, CS_I_MP2 case (red curve) and CS_I_MP3 case (blue curve), compared to the corresponding observed daily maximum (red crosses) and minimum values (light blue crosses): Astore, top left; Skardu, top right; Gilgit, bottom left; Bunji, bottom right

two different microphysics schemes. In correspondence to the temperature trend, the simulated relative humidity trends also start differentiating especially after the 28th of July at 12:00 UTC. While the CS_I_MP2 simulated relative humidity values maintain a regular daily cycle, in agreement with the corresponding temperature, CS_I_MP3 shows a different trend, responding to the flood perturbation as analogously seen for its temperature. As expected, during the flood the CS_I_MP3 relative humidity loses the diurnal cycle and keeps high and almost constant values. At Astore, Gilgit and Bunji the differences between the two microphysics schemes are larger than at Skardu station, where the difference in the trends starts even later, on the 29th of July.

Since only the microphysics parameterization is different in the two runs, the larger perturbations in the temperature and in the relative humidity produced in the CS_I_MP3
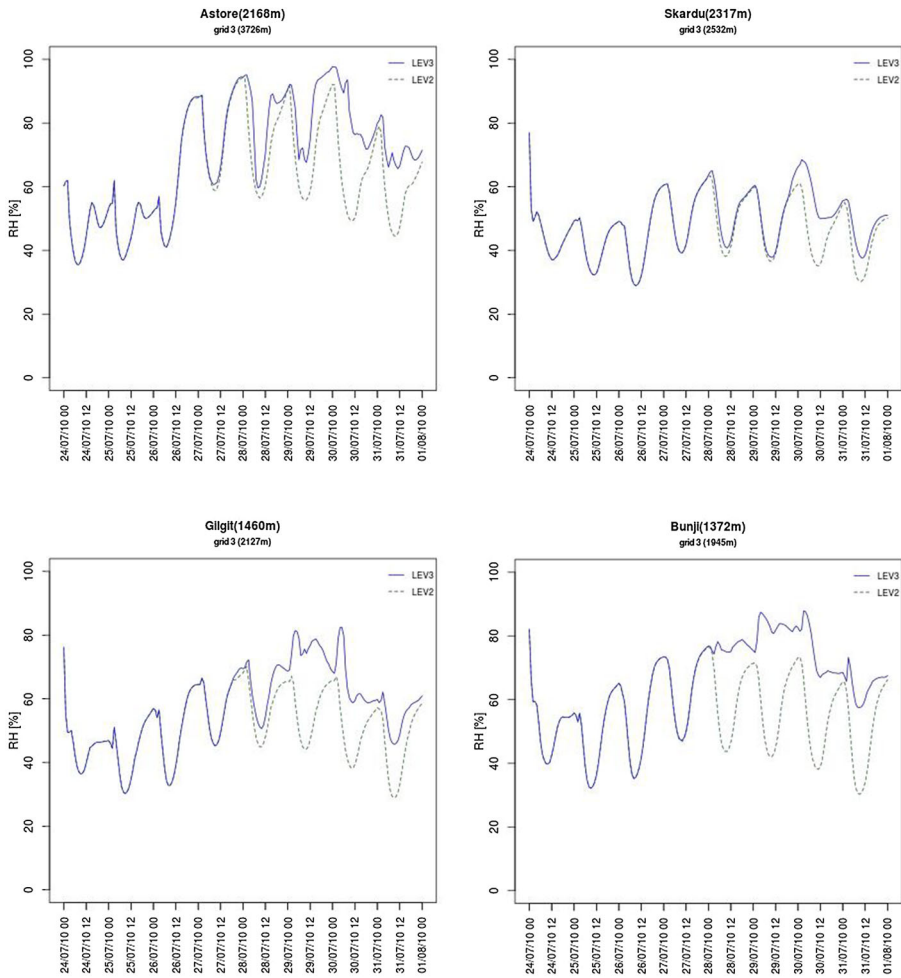
Fig. 3 Case Study I. Grid 3. Time evolution of the simulated relative humidity at one of the grid point closest to the PMD stations using two different microphysics parameterizations, CS_I_MP2 case (green curve) and CS_I_MP3 case (blue curve): Astore, top left; Skardu, top right; Gilgit, bottom left; Bunji, bottom right. Observed data were not available

simulation are linked to the intense precipitation event, occurring between the 29.07 and 01.08.

In Fig. 4, the resolved surface precipitation at the two grid points for CS_I_MP3 is plot together with the value interpolated at the station. We notice that for CS_I_MP2 option no precipitation is computed. Observed mean-daily values at the four PMD stations were available and are plotted as reference. Since two different variables are considered, the comparison has to be taken in a qualitative way, examining whether the model predicts the precipitation episode. The model correctly forecasts the intense precipitation event, in terms of period (last days of July). The predicted resolved surface precipitation shows lower values than the observed daily mean. The dislocation of the grid points with respect to the actual position of the station may contribute to the difference, since precipitation is a
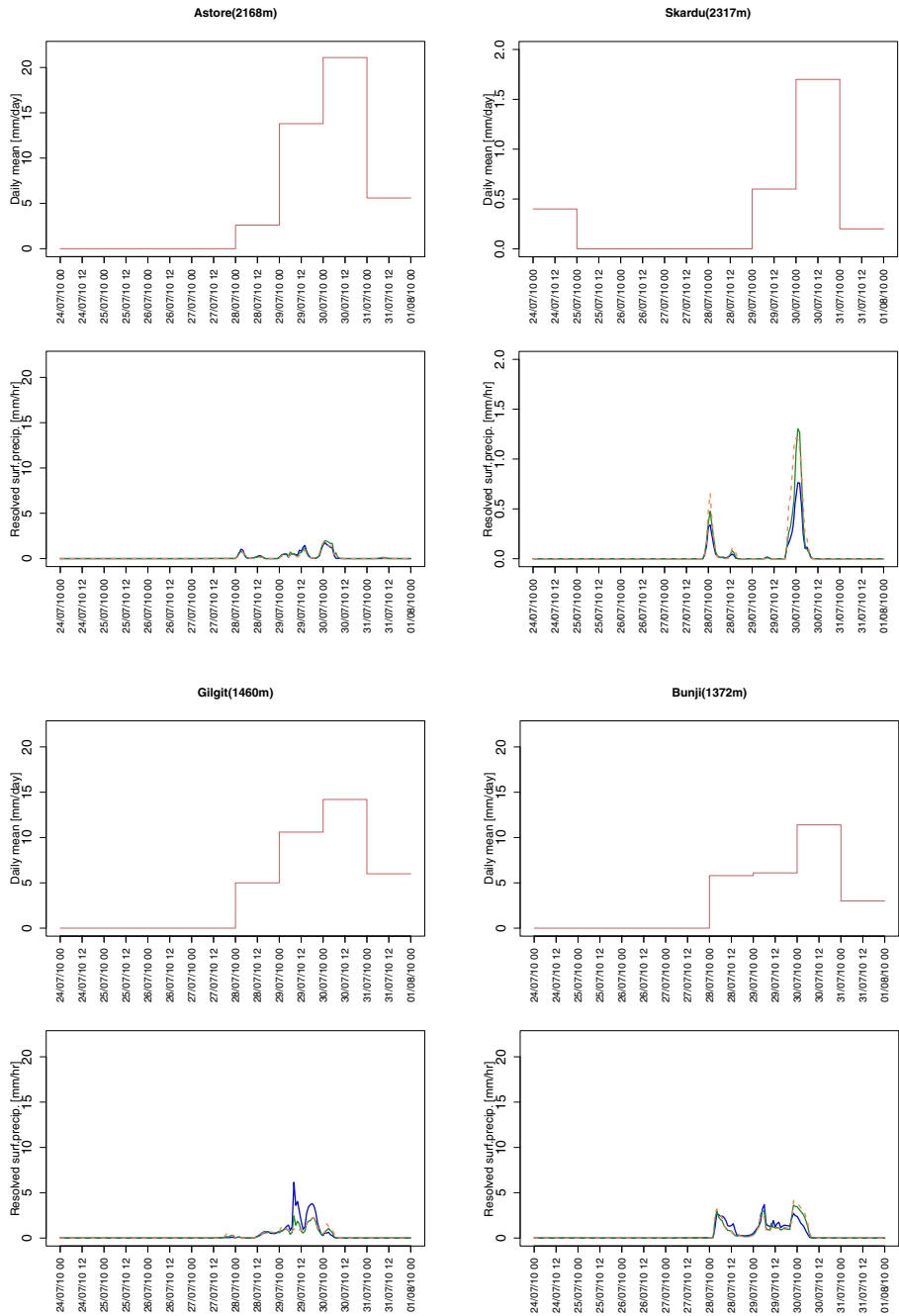
Fig. 4 Case Study I. Grid 3, CS_I_MP3 case. Observed mean daily precipitation values (red line, upper panels) and time evolution of the simulated resolved precipitation (lower panels) at the two grid points closest to the PMD stations (blue and green lines) and interpolated at the station (red dashed line): Astore, top left; Skardu, top right; Gilgit, bottom left; Bunji, bottom right

rather local variable and may largely vary over distances of 1-km order. We note that the values of the precipitation in Skardu are an order of magnitude lower than at the other stations (see the scale in Fig. 4). Together with the results for the temperature and humidity, this confirms that both the heat wave and the flood episode affected Skardu location to a lesser extent. Since the agreement between simulated and observed fields is better at Skardu station, we may infer that in less perturbed conditions the model produces meteorological fields that are reasonably representative of the atmospheric conditions in the area.

The results of Case Study I highlight the importance of adopting an advanced micro-physics parameterization, not only for being able to capture precipitation events, but also for the consequent correct reproduction of the temperature and humidity fields.

## 4 Case Study II: model performance in complex terrain at different resolutions

In the period between the 20th of August and the 10th of November 2012 experimental campaigns were carried out at Askole [15], to provide a first indication of the variability of the atmospheric composition as a function of the atmospheric circulation and to investigate the levels of aerosol and reactive gases in the Karakorum area, where no information existed. The choice of Askole location was also linked to the possibility of analysing the role of the along-valley thermal circulation, investigating the influence of local emissions and long-range transport. For this period, we had available observed meteorological data that can thus support a quantitative evaluation of the model results. This case study is aimed at assessing the capability of the model to reproduce the atmospheric conditions and to provide reliable high-resolution meteorological fields that can be used as input to air pollutant dispersion studies. In fact, the atmospheric pollution is determined by specific physical processes and possible problems, related to the particular features that both meteorological and dispersive processes assume in complex topography. As anticipated in the introduction, several studies in real complex terrain demonstrated that typical terrain-induced meteorological processes cannot be correctly captured when using resolutions coarser than 1 km. Already at resolutions of 3–4 km, model forecasts can happen to deviate substantially from the observations.

Citing Putero et al. [15], the wind speed during the field campaign had a rather low average value (2.2 ± 1.4 m s^{-1}), the local wind being strongly affected by the development of thermal circulation along the valley. The observed wind directions showed a bidirectional distribution with dominating directions from East and West of the valley. The diurnal variation of the wind was characterized by westerly up-valley winds during the day and easterly down-valley winds during night time (wind speed > 2.5 m s^{-1} coming from SW in central day hours; wind speed 1.3–2.5 m s^{-1} coming from E–NE during the remaining day hours).

RAMS simulations were run for a ten-day period, from the 25.08 to 05.09.2012 included. The same configuration of RAMS model as depicted in Table 1 was used, simulations were performed considering the same topography smoothing and microphysics parameterization as in test case CS_I_MP3.

The RAMS simulated fields were extracted from the analysis files at the first level, 24 m, of the four grid points around the station, identified as SW = South-West, NW = North-West, SE = South-East, NE = North-East. In Figs. 5, 6 and 7 we plot
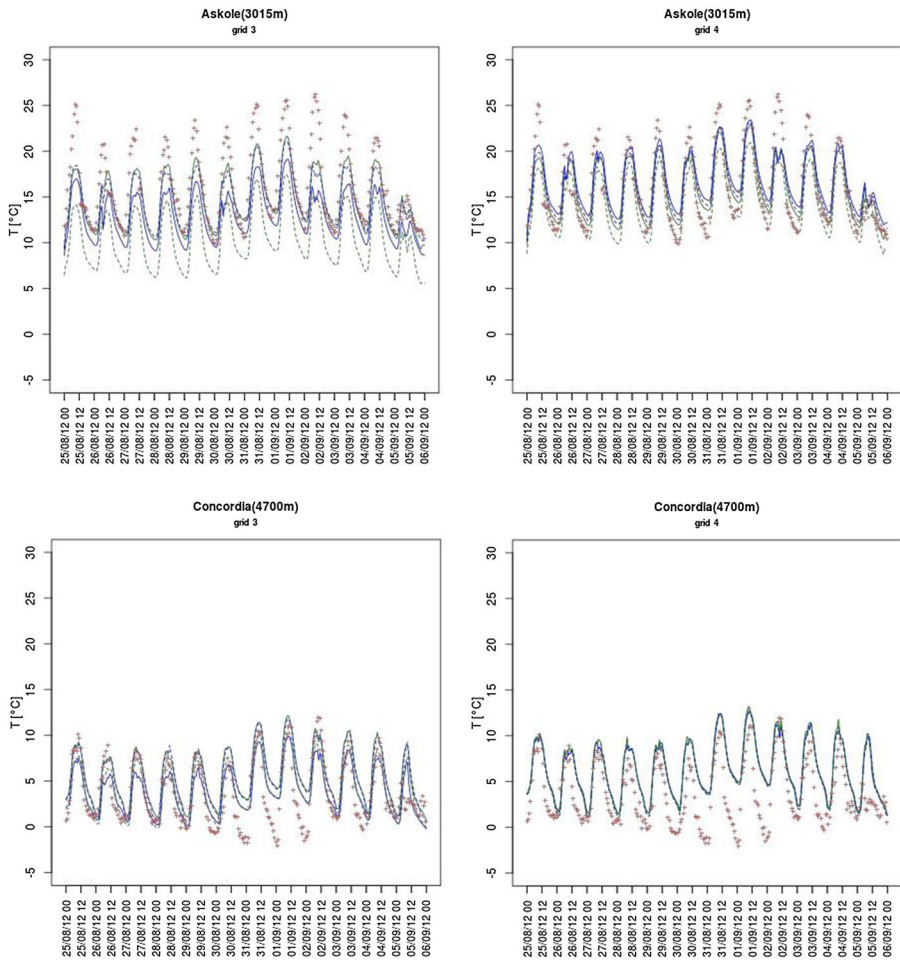
Fig. 5 Case Study II. Time evolution of the simulated temperature at the four grid points closest to the Askole (top) and Concordia (bottom) stations (SW blue line, SE green line, NW blue dashed line, NE green dashed line), compared to the corresponding observed values (red crosses) in Grid 3 (left) and Grid 4 (right)

respectively the temperature, the relative humidity and the wind speed observed and predicted at Askole and Concordia for Grids 3 and 4.

Based on a qualitative comparison, the agreement between predicted and observed temperature looks relatively fair for both Grids 3 and 4. It is worth noticing that the spreading of the curves at the four points reduces in Grid 4 thanks to the finer resolution, with the altitudes of the grid points being closer to the site one, thus more representative of the local features. At Askole the model well captures the timing of the daily cycle and the minimum temperature values, while it misses the maxima. The sensible improvement obtained with the finest resolution and the non-negligible differences even among the values simulated at the adjacent grid points suggests that the discrepancy may be connected to the displacement of their positions with respect to the measuring site. Being set on a slope, different exposure to the sun rays and the shadows cast may influence the temperature values at different points, and these effects add on the different heights of the
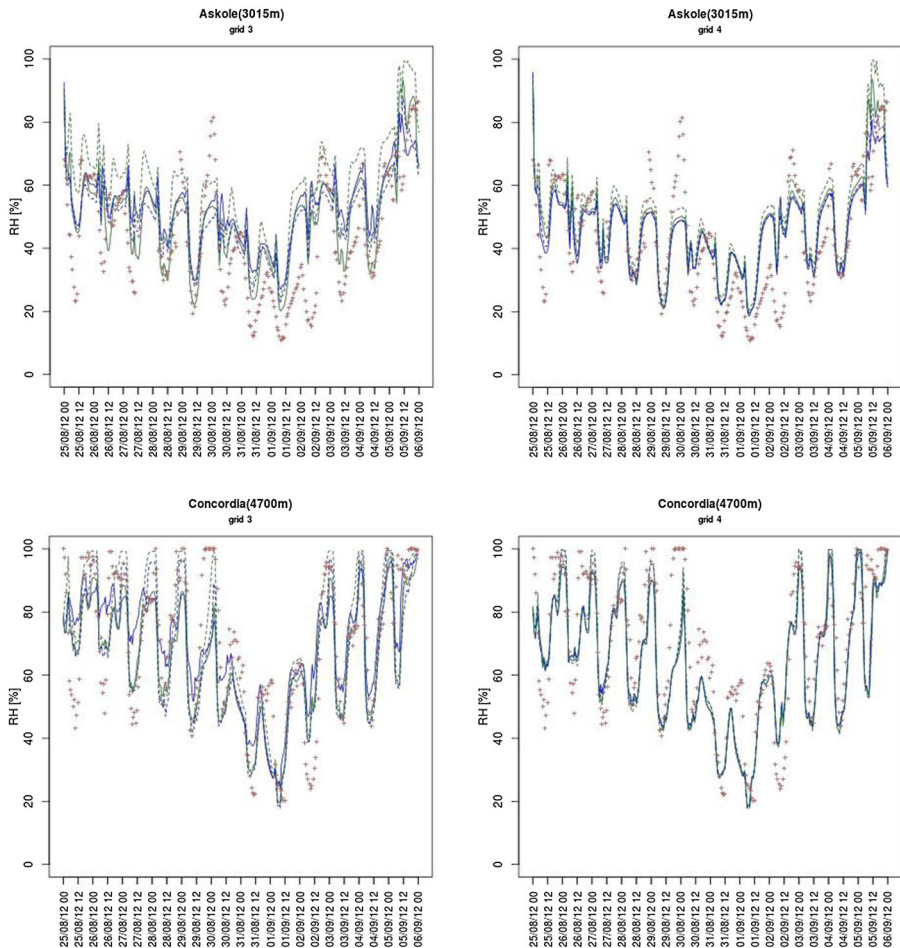
Fig. 6 As in Fig. 5 but for the relative humidity

measured (2 m) and the simulated (24 m) data. In Concordia the daily variation is well reproduced in the first 5 and last 3 days, but the simulation cannot fully capture the large temperature excursion and the fast decrease of the values, recorded by the observations from August 31st to September 2nd. The humidity is rather well predicted in both Grids, the variation seen for the temperature from August 31st and September 2nd mirrors in the humidity field, which assumes lower values. The increase in the observed temperature during the day and the decrease in the night, together with the decrease in humidity, indicate that those days are characterized by clear sky conditions, differently than the trend in previous and following period, in particular at Concordia station. Here, the temperature minima in the night are not correctly reproduced; in the simulation the ongoing long-wave radiation process from the ground seems much less effective. This might be due to low-level clouds simulated by the model above the site. Snow cover can contribute to the reduction of temperature minima as observed, and concurrently it is a critical quantity for model simulation. The simulation generally well represents the wind speed daily trend but some overestimation of the values is produced at the NE and SE grid points, in particular
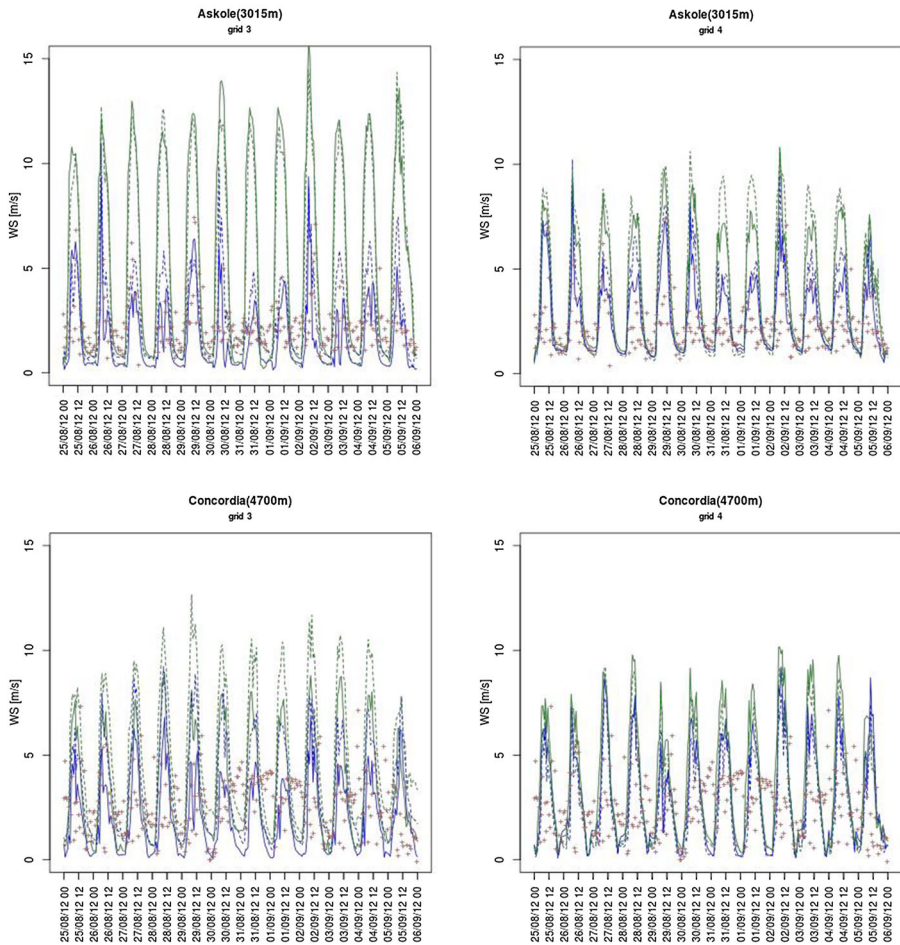
Fig. 7 As in Fig. 5 but for the wind speed

for Grid 3. The overestimation may be related to the different altitudes of the grid points and the station and to the different level at which the data are considered, 10 m for the observations and 24 m for the predictions. Generally, taking into account that the spacing for Grid 3 is 4 km and that the points have different altitudes with respect to the measuring station, the model results can be considered already fair at this resolution in some points. The agreement between predictions and observations further improves in Grid 4. The wind speed shows a certain scatter between the values at the different grid points, of course larger for the coarser grid. The predicted values better match the observed data for Grid 4, as for the other variables, and the scatter largely reduces. Clearly, when increasing the resolution the meteorological variables at nearby grid points get closer values. The differences between predictions and observations may be ascribed to the intrinsic limitation of a model in fully reproducing the specific and localized characteristics caught by the observed data. Even so, the quality of the results confirm that the application of a mesoscale models at high resolution can provide reliable fields and an effective description of the local atmospheric circulation also in highly complex terrain. In fact, we note that the

two case studies here considered are related to extreme events and critical conditions. Thus, we may expect the model to meet its limit even at the relatively fine resolution adopted for the simulations. On the other hand, when the conditions are less disturbed, the agreement with the observations is fair, as in Figs. 5 and 6 when looking at the first and last days of the simulated period.

Connected to the sensitivity to grid resolution, a problem may arise when comparing predicted and observed data at measured stations by interpolating the values obtained at surrounding grid-points. While this approach can be acceptable in homogeneous terrain, as noted before it becomes not straight applicable in complex orography since values at rather different altitudes might be improperly interpolated. This is a known problem, yet interpolated values are commonly used as representative of the meteorological variables at sites of interest. Therefore, when there is the need to obtain variables interpolated on the location of a measuring station, having finer grids makes the comparison more reliable.

To assess this aspect, we compared paired values, estimating the predicted variable by interpolation from the values at the grid points surrounding the station, for both Grids 3 and 4. The agreement generally improves for Askole in Grid 4, in particular for the temperature but also for the relative humidity, while the wind speed is less sensitive to the different resolution and the improvement regards mostly the lower wind speeds. We found a substantial underestimation of the interpolated temperature at Askole in Grid 3, which may be related to its position on a mountain slope, since values at distant points down- and up-slope can be very different. In fact, the altitude of the interpolated point in Grid 3 is much higher than the actual altitude of the station (see Table 3). At Concordia, the agreement for the temperature instead is better for Grid 3 than for Grid 4, where the 1-km resolution simulation shows a tendency to overestimate the measured data. The scatter of the relative humidity reduces in Grid 4 and the wind speed takes lower values than in Grid 3. The altitude of the interpolated point for Concordia is respectively higher in Grid 3 and lower in Grid 4 with respect to the actual height (Table 3). We cite that two of the Grid 3 points around Concordia have very close altitude to the site, 4752 m for the NW point and 4775 m for the SE. In addition, the NW point is also close in latitude and longitude. Instead, all Grid 4 points around the site have a lower altitude. Thus, in this case it happens that the interpolated variables in Grid 3 are more representative of a mountaintop station than the correspondent values in Grid 4.

As expected, the agreement is generally better for Grid 4 when comparing the trends of the interpolated variables with the values at the four grid points (not shown). In particular, in some cases for Grid 3 the weighted contributions from the grid-points that are more distant from the station location, thus less representative of its meteorology, deteriorate the agreement with the observations.

This analysis described the possible criticality in considering interpolated simulated values to study the atmospheric conditions at a specific site in complex terrain. Increasing the horizontal resolution and using interpolated values not always ensure the representativeness of the predicted data in complex orography, where the altitude plays a key role. It is thus necessary to consider carefully the topographical characteristics of the area in order to compare paired predicted and observed variables with a sound approach, evaluating the reliability of the interpolation or choosing the most representative grid point to refer to.

To provide an estimate of the deviation of the predicted values with respect to the observations, we calculated a few metrics, even if we need to consider that the number of pairs is relatively small, 274 for Askole and 289 for Concordia stations: the normalized mean square error (NMSE), fractional bias (FB) and factor of two (FA2),

Table 4 Askole station, statistics for wind speed, temperature and relative humidity, for Grid 3 (G3) and Grid 4 (G4)

Askole		Wind speed			Temperature			Relative humidity		
		NMSE	FB	FA2	NMSE	FB	FA2	NMSE	FB	FA2
Interp. point	G3	1.02	− 0.40	0.41	0.59	0.70	0.38	0.23	− 0.41	0.75
	G4	0.89	− 0.52	0.61	0.01	0.02	1.00	0.07	− 0.08	0.97
SW point	G3	0.78	0.30	0.42	0.07	0.22	1.00	0.11	− 0.10	0.87
	G4	0.51	0.10	0.65	0.02	− 0.04	1.00	0.07	− 0.04	0.98
SE point	G3	0.85	− 0.31	0.39	0.02	0.10	1.00	0.08	− 0.13	0.96
	G4	0.60	− 0.36	0.67	0.01	0.02	1.00	0.07	− 0.08	0.97
NW point	G3	0.62	0.18	0.44	0.03	0.10	1.00	0.09	− 0.13	0.93
	G4	0.44	− 0.10	0.71	0.02	− 0.01	1.00	0.07	− 0.06	0.97
NE point	G3	1.07	− 0.42	0.35	0.21	0.42	0.99	0.14	− 0.30	0.85
	G4	0.89	− 0.48	0.57	0.03	0.12	1.00	0.09	− 0.15	0.94

Table 5 As in Table 4 but for Concordia station

Concordia		Wind speed			Temperature			Relative humidity		
		NMSE	FB	FA2	NMSE	FB	FA2	NMSE	FB	FA2
Interp. point	G3	1.0	− 0.52	0.47	0.22	− 0.13	0.65	0.04	0.03	0.99
	G4	0.89	− 0.13	0.50	0.47	− 0.54	0.53	0.05	0.09	0.99
SW point	G3	0.86	0.10	0.45	0.25	− 0.05	0.71	0.05	0.001	0.98
	G4	0.86	− 0.11	0.51	0.46	− 0.53	0.53	0.05	0.09	0.99
SE point	G3	0.78	− 0.01	0.47	0.33	− 0.40	0.62	0.04	0.08	0.99
	G4	0.89	− 0.22	0.47	0.46	− 0.54	0.54	0.05	0.09	0.99
NW point	G3	0.82	− 0.17	0.49	0.32	− 0.37	0.62	0.04	0.07	0.99
	G4	0.93	0.01	0.45	0.42	− 0.49	0.56	0.04	0.08	1.00
NE point	G3	0.92	− 0.16	0.39	0.23	− 0.10	0.63	0.03	− 0.01	0.99
	G4	0.88	− 0.05	0.46	0.45	− 0.53	0.55	0.05	0.08	1.00

$$NMSE = \frac{1}{N} \sum_i \frac{(\phi_{pi} - \phi_{oi})^2}{\bar{\phi}_o \bar{\phi}_p} \tag{1}$$

$$FB = 2 \frac{\bar{\phi}_o - \bar{\phi}_p}{\bar{\phi}_o + \bar{\phi}_p} \tag{2}$$

$$FA2 = \text{ Fraction of data that satisfy the condition } 0.5 \leq \frac{\phi_{pi}}{\phi_{oi}} \leq 2.0 \tag{3}$$

where ϕ represents a generic variable and subscripts 'o' and 'p' stand respectively for 'observed' and 'predicted'. The FB is a measure of the mean bias and the NMSE provides a measure of the scatter. The statistics are calculated for Grids 3 and 4, both for the interpolated values and for the four grid points around the location of the station in the simulation domain, and are reported in Table 4 for Askole and Table 5 for Concordia.

The values of the metrics conform to typical statistical evaluations of mesoscale models in complex terrain (see for instance Gross [9]).

The statistics confirm that for Askole when passing from Grid 3 to Grid 4 there is a general improvement in the agreement between predictions and observations, in particular for the temperature and for the interpolated value. In Concordia, there is only a slight improvement for the wind speed, while the agreement does not practically change for the relative humidity. The agreement for the temperature gets even a bit worse in Grid 4, where the FB values indicate a general overestimation of the observed values, as already highlighted in previous Fig. 5, especially for the period between 31.08 and 02.09.2012. In Askole the metrics of the interpolated point are generally worse than those calculated at the grid points, while in Concordia they are more similar, especially for temperature and humidity. In any case, when evaluating the performances of the model against measurements, for which here a quality index is not given, we need to take into account the issues discussed in the introduction and also that the period considered for the comparison in this case study is short.

In Fig. 8 we plot the wind direction as reproduced at the four grid points around Askole site, in Grids 3 and 4. As usual, a larger spread of the predicted data characterize Grid 3, while in Grid 4 the curves at the four points are mostly similar. The agreement with the observed direction is rather poor in this case. The observed data show a bi-modal trend, instead the predicted values vary only between 200 and 250 degrees for Grid 4, while in Grid 3 the variability is a bit better captured. To have a more comprehensive description, we calculated the wind speed and direction averaged over the full period of Case Study II as a function of the hour of the day. In Fig. 9 we show the plots for the observations and for the predicted fields as calculated through the interpolation over the station site and as
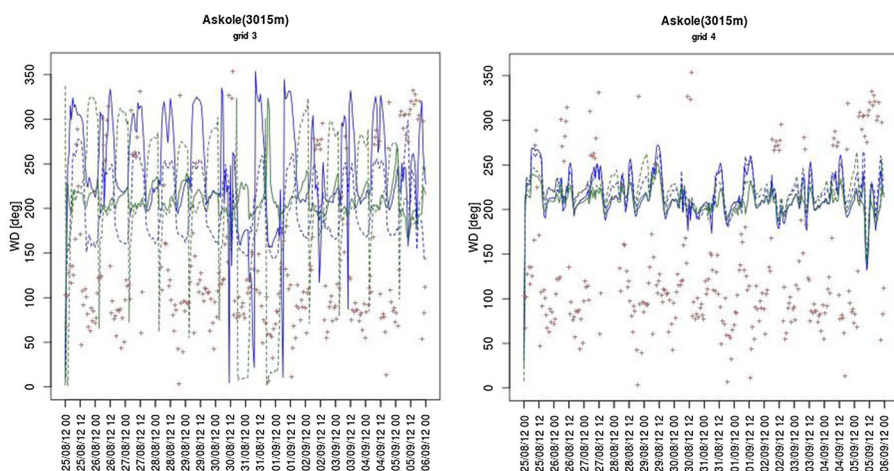

Fig. 8 Case Study II. Time evolution of the wind direction values at the four grid points closest to Askole station (SW blue line, SE green line, NW blue dashed line, NE green dashed line), on grid 3 (left) and grid 4 (right), compared to the observed values (red crosses)
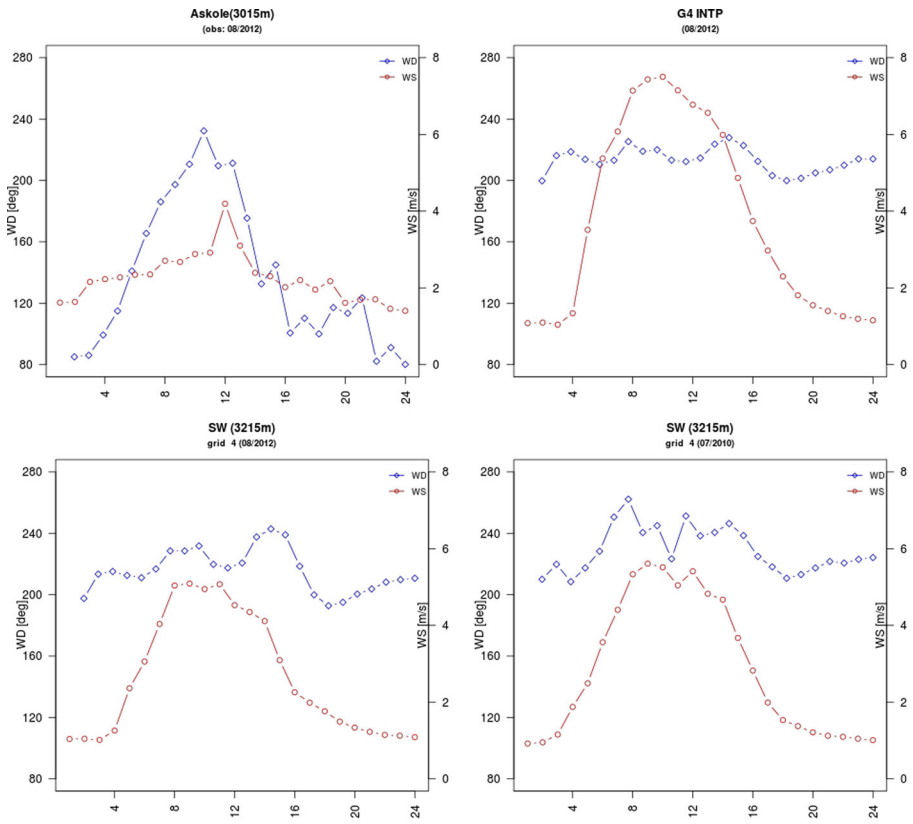
Fig. 9 Case Study II. Daily trend of the average wind speed (red circles) and direction (blue diamonds) measured at Askole station (top left), and as simulated: interpolated on Grid 4 (top right), extracted at the SW grid point (bottom left). Corresponding values for the July period in Case Study I, at SW grid point (bottom right)

extracted at the closest SW grid point. We add also the plot of the predicted fields for the period considered in Case Study I at the SW grid point, for comparison. The wind speed data interpolated on the measurement site show larger values than those observed and predicted at the closest SW grid point. In all cases, the predicted wind speed shows a very clear daily cycle, with maxima during the afternoon between 1 and 5 p.m. local time, and the wind direction is confirmed to vary in a limited sector, 200–250 degrees. Also the observations show a daily cycle for the wind speed, less peaked and variable but in the same time interval, and the bi-modal direction is revealed, with a main peak between 200° and 240° and a second peak around 120°. The behaviour of the simulation becomes clear looking at the wind roses plotted on the orography, as in Fig. 10 for Grid 4 (see the Online Resources for the correspondent Figure SM3 related to Grid 3). RAMS simulations are strongly characterized by the valley-mountain circulation, while observations describe more along-valley, slope winds and local circulation. In previous studies in complex terrain, we generally obtained a good reproduction of the wind direction using RAMS model [23, 24, 26]. The poor performance in this case might be related to the particular location of the monitoring station, on a plateau set on a slope that rises up both along and crosswise the valley directions, ending against a cliff edge (see Figure SM4 in the Online
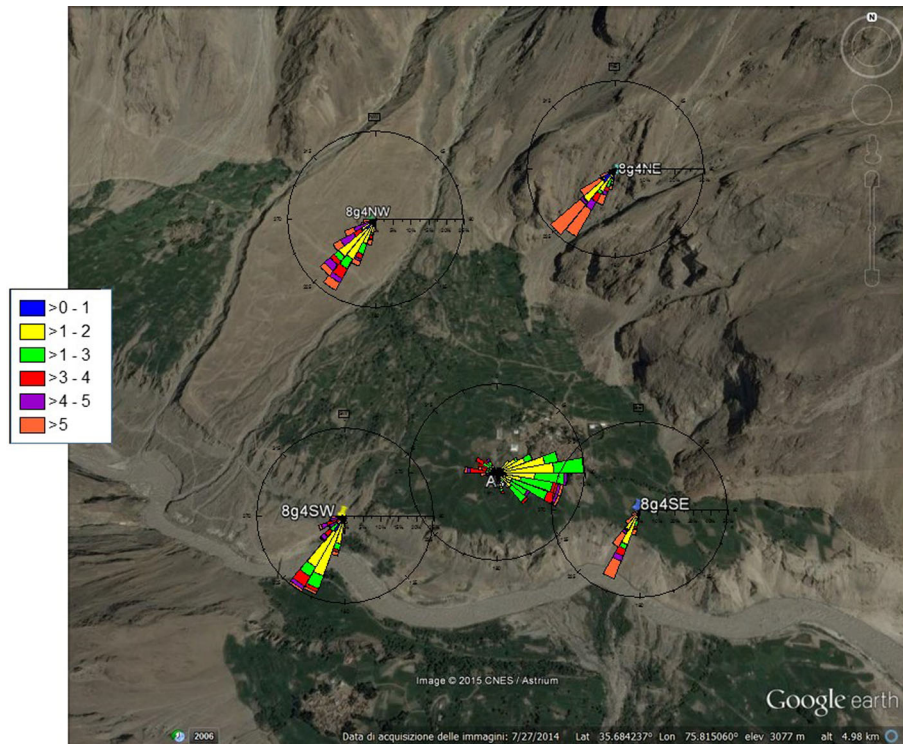
Fig. 10 Case Study II. Grid 4. Wind roses at the Askole station (A) and at the four grid points around it

Resources). At 1-km resolution, the model can hardly be able to reproduce these details in the orography and to solve the specific local circulation. The differences in the slope orientation and steepness between the model grid points and the site may as well affect and weaken the agreement between predictions and observations. This result seems to indicate that even at high resolutions, in such highly complex topography the local specific circulation may be scarcely depicted by mesoscale models, which are more representative of the regional-scale processes. However, analysing the diurnal behaviour of the aerosol concentration, Putero et al. [15] could observe that in daytime particles from the lower troposphere were transported to Askole by up-valley thermal circulation, while during night-time cleaner air masses were transported by down-valley winds. Their result supports and highlights the importance of the valley-mountain circulation, which instead might be not captured by the local point measurements.

5 Conclusions

RAMS numerical modelling experiments at high-resolution have been performed to simulate relevant physical and dynamical processes in the highly complex topography of the Hindu Kush-Karakorum-Himalaya (HKKH) region. The rationale of this work, which is part of an extensive research project, was to discuss some critical aspects when performing simulation of the atmospheric circulation in very inhomogeneous topographical conditions.

Physical and numerical aspects have been considered and studied on the modelling point of view. The results have been analysed comparing different parameterizations and have been evaluated using available observations at some measuring stations in the area.

RAMS model was applied using four nested grids, thus reaching a high resolution, up to 1 km for the smallest grid spacing. Previous studies in the European Alpine region focused on the sensitivity to the input data, to the grid resolution and to downscaling procedures between prognostic and diagnostic mass-consistent models [2, 26]. Atmospheric boundary-layer parameterizations and turbulence closures were investigated in mountainous terrain, both in coastal Japanese areas [10, 24] and in the Italian Alps [2, 25]. Here, the sensitivity to the smoothing of the orography in the model simulation was addressed and discussed, quantifying its effect on the simulated variables. It was shown that even small differences in the topography may lead to non-negligible differences in the wind field. The effect of the microphysics parameterization in application to heavy rain events was investigated. The necessity of adopting advanced parameterizations, which are essential for correctly representing the temperature and humidity fields, especially to capture precipitation events, was assessed. When estimating atmospheric variables by interpolation of simulated values at a site of interest, the simulation grid spacing is a key factor. In the present work the deviation from the observed variables was quantified for coarser and finer resolutions, considering grid meshes of 4 km and 1 km. It was shown that, particularly in complex orography, when variables need to be provided on a specific location by interpolation, using finer grids and higher resolutions is a fundamental requirement to provide more reliable values. However, given the variability in altitudes, not always higher resolutions ensure that the interpolated variables are effectively representative of the meteorology at a site. While high-resolution interpolation can give appropriate weighted values on slopes, at mountaintops values from points at lower altitudes may spoil the estimation of the atmospheric variables at the site.

In principle, an order of 1-km resolution for simulations can still be too coarse for correctly reproducing the local atmospheric circulation in highly complex terrain. However, the quality of the comparison between predicted and observed data and its related statistical quantification, showed that a mesoscale model like RAMS can be considered a tool reliable enough for estimating the meteorological variables in such very complex orography as in HKKH area. Even in extreme conditions, like for the flood episode occurred in July 2010 and for the transient meteorological conditions in August 2012. Indeed, in such perturbed conditions the model meets its limits. Taking into account the intrinsic limitations related to the grid resolution and that in unperturbed conditions the simulated fields fairly agree with the observed variables, the model predictions can be retained adequately accurate, also considering the critical aspects associated to a paired comparison with observations. The sensitivity analyses carried out showed that the choice of the parameterizations are, as expected, key items for an appropriate reproduction of the meteorological fields. Even at 1-km resolution, the outputs of the model keep being more representative of the regional-scale atmospheric processes and reproduce the main typical features of the mountainous circulations, missing the most local characteristics and effects observed at single sites. In any case, the outputs of the simulations are robust enough to be representative of the regional circulation in the area.

References

1. Arnold D, Morton D, Schicker I, Seibert P, Rotach MW, Horvath K, Dudhia J, Satomura T, Müller M, Zängl G, Takemi T, Serafin S, Schmidli J, Schneider S (2012) High resolution modelling in complex terrain. Report on the HiRCoT 2012 Workshop, Vienna, 21–23 February 2012. BOKU-Met Report 21, p 42. ISSN 1994-4179 (Print), ISSN 1994-4187 (Online). http://www.boku.ac.at/met/report/BOKU-Met_Report_21_online.pdf

2. Balanzino A, Trini Castelli S (2015) Critical issues for meteorological simulations with high resolution in very complex topography. D2.5.R.1b Report Special Project RECCO, NextData Project. http://www.nextdataproject.it/?q=en/content/d25r1b-critical-issues-meteorological-simulations-high-resolution-very-complex-topography, p 50

3. Binder P, Schär C (eds) (1996) MAP design proposal. MeteoSwiss, p 75. [Available from the MAP Programme Office, Meteo- Swiss, CH-8044, Zurich, Switzerland.]

4. Cotton WR, Pielke RA, Walko RL, Liston GE, Tremback CJ, Jiang H, McAnnelly RL, Harrington JY, Nicholls ME, Carrio GG, McFadden JP (2003) RAMS 2001: current status and future directions. Meteorol Atmos Phys 82:5–29

5. De Wekker SFJ, Steyn DG, Fast JD, Rotach MW, Zhong S (2005) The performance of RAMS in representing the convective boundary layer structure in a very steep valley. Environ Fluid Mech 5:35–62

6. Galarneau TJ Jr, Hamill TM, Dole RM, Perlwitz J (2012) A multiscale analysis of the extreme weather events over western Russia and northern Pakistan during July 2010. Mon Weather Rev 140(5):1639–1664

7. Gohm A, Zängl G, Geier G (2003) South foehn in the Wipp Valley on 24 October 1999 (MAP IOP 10): verification of high-resolution numerical simulations with observations. Mon Weather Rev 132:78–102

8. Grell GA, Dudhia J, Stauffer DR (1995) A description of the fifth generation Penn State/NCAR mesoscale model (MM5). NCAR Tech. Note NCAR/TN-3981STR, p 122

9. Gross G (1994) Statistical evaluation of the mesoscale model results. In: Pielke RA, Pearce RT (eds) Mesoscale modeling of the atmosphere, meteorol. monogr, vol 25, no 47, Am. Meteorol. Soc., Boston, pp 137–154

10. Hara T, Trini Castelli S, Ohba R, Tremback CJ (2009) Validation studies of turbulence closure schemes for high resolutions in mesoscale meteorological models—a case of gas dispersion at the local scale. Atmos Environ 43:3745–3753

11. Heimann D, de Franceschi M, Emeis S, Lercher P, Seibert P, Anfossi D, Antonacci G, Baulac M, Belfiore G, Botteldooren D, Cemin A, Clemente M, Cocarta D, Defrance J, Elampe E, Forkel R, Grießer E, Krüger B, Miège B, Obleitner F, Olny X, Ragazzi M, Rüdisser J, Schäfer K, Schicker I, Suppan P, Trini Castelli S, Uhrner U, Van Renterghem T, Vergeiner J, Zardi D (2007) Air pollution, traffic noise and related health effects in the Alpine space: a guide for authorities and consulters. ALPNAP Comprehensive Report, Università degli Studi di Trento, Dipartimento di Ingegneria Civile e Ambientale, Trento, Italy, p 335

12. Houze RA Jr, Rasmussen KL, Medina S, Brodzik SR, Romatschke U (2011) Anomalous atmospheric events leading to the summer 2010 floods in Pakistan. Bull Am Meteorol Soc 92:291–298

13. Mesinger F, Janjic ZI, Nickovic S, Gavrilov D, Deaven DG (1988) The stepmountain coordinate: model description and performance for cases of Alpine lee cyclogenesis and for a case of an Appalachian redevelopment. Mon Weather Rev 116:1493–1518

14. Pielke RA, Cotton WR, Walko RL, Tremback CJ, Lyons WA, Grasso LD, Nicholls ME, Moran MD, Wesley DA, Lee TJ, Copeland JH (1992) A comprehensive meteorological modeling system—RAMS. Meteorol Atmos Phys 49:69–91

15. Putero D, Cristofanelli P, Laj P, Marinoni A, Villani P, Broquet A, Alborghetti M, Bonafè U, Calzolari F, Duchi R, Landi TC, Verza GP, Vuillermoz E, Bonasoni P (2014) New atmospheric composition observations in the Karakorum region: influence of local emissions and large-scale circulation during a summer field campaign. Atmos Environ 97:75–82

16. Regmi RP, Kitada T, Kurata G (2003) Numerical simulation of late wintertime local flows in Kathmandu valley, Nepal: implication for air pollution transport. J Appl Meteorol 42:389–403

17. Rotach MW, Calanca P, Graziani G, Gurtz J, Steyn DG, Vogt R, Andretta M, Christen A, Cieslik S, Connolly R, De Wekker SFJ, Galmarini S, Kadygrov EN, Kadygrov V, Miller E, Neininger B, Rucker M, van Gorsel E, Weber H, Weiss A, Zappa M (2004) Turbulence structure and exchange processes in an Alpine valley: the Riviera project. Bull Am Meteorol Soc 85:1367–1385

18. Rotach MW, Zardi D (2007) On the boundary layer structure over highly complex terrain: key findings from MAP. Q J R Meteorol Soc 133:937–948. https://doi.org/10.1002/qj.71

19. Schicker I, Seibert P (2009) Simulation of the meteorological conditions during a winter smog episode in the Inn Valley. Meteorol Atmos Phys 103:211–222

20. Skamarock WC et al (2008) A description of the advanced research WRF version 3. NCAR Tech. Note NCAR/TN-4751STR, p 113. http://www.mmm.ucar.edu/wrf/users/docs/arw_v3_bw.pdf
21. TRACT Special Issue (1998) Atmospheric environment 32(7)
22. Trenberth KE, Fasullo JT (2012) Climate extremes and climate change: the Russian heat wave and other climate extremes of 2010. J Geophys Res 117:D17103. https://doi.org/10.1029/2012JD018020
23. Trini Castelli S, Morelli S, Anfossi D, Carvalho J, Zauli Sajani S (2004) Intercomparison of two models, ETA and RAMS, with TRACT field campaign data. Environ Fluid Mech 4:157–196
24. Trini Castelli S, Hara T, Ohba R, Tremback CJ (2006) Validation studies of turbulence closure schemes for high resolutions in mesoscale meteorological models. Atmos Environ 40:2510–2523
25. Trini Castelli S, Anfossi D, Belfiore G (2008) Inclusion of a turbulence parameterisation in a diagnostic mass consistent model driven by a prognostic model. In: Proceedings of the 12th international conference on harmonisation within atmospheric dispersion modelling for regulatory purposes, Cavtat, Croatia, 6–9 October 2008, Hrv. Meteor. Časopis Ed. vol 43, pp 254–258. ISSN: 1330-0083
26. Trini Castelli S, Belfiore G, Anfossi D (2011) Modelling the meteorology and traffic pollutant dispersion in highly complex terrain: the ALPNAP Alpine Space Project. Int J Environ Pollut 44((1/2/3/4)):235–243
27. Wagner JS, Gohm A, Rotach MW (2014) The impact of horizontal model grid resolution on the boundary layer structure over an idealized valley. Mon Weather Rev 142(9):3446–3465
28. Wang S-Y, Davies RE, Huang W-R, Gillies RR (2011) Pakistan's two-stage monsoon and links with the recent climate change. J. Geophys Res 116:D16114. https://doi.org/10.1029/2011JD015760
29. Walko RL, Tremback CJ (2006) Regional atmospheric modeling system—version 6.0—MODEL INPUT NAMELIST PARAMETERS. Document Edition 1.4, October 2006. http://www.atmet.com/html/docs/rams/ug60-model-namelist-1.4.pdf. Accessed 15 Jan 2016)
30. Zängl G, Egger J, Wirth V (2001) Diurnal winds in the Himalayan Kali Gandaki Valley. Part II: Modeling. Mon Weather Rev 129:1062–1080
31. Zängl G, Gohm A, Geier G (2004) South foehn in the Wipp Valley—Innsbruck region: numerical simulations of the 24 October 1999 case (MAP-IOP 10). Meteorol Atmos Phys 86:213–243